Cancer Research

Mesenchymal Stem Cell–Derived Exosomes Stimulate Cycling Quiescence and Early Breast Cancer Dormancy in Bone Marrow

Sarah A. Bliss[1,2], Garima Sinha[1,2], Oleta A. Sandiford[1], Lisa M. Williams[1,2], Daniel J. Engelberth[1,2], Khadidiatou Guiro[1], Leidy L. Isenalumhe[3], Steven J. Greco[1], Seda Ayer[1], Margarette Bryan[1], Rakesh Kumar[4], Nicholas M. Ponzio[5], and Pranela Rameshwar[1,2]

Abstract

Dormant breast cancers resurge as metastatic disease after a long dormancy period in the bone marrow, where cancer cells interact with mesenchymal stem cells (MSC). However, the nature of early interactions between breast cancer cells and MSCs in the bone marrow microenvironment that facilitate adaptation to a quiescent state remains poorly understood. Here, we report that breast cancer cells prime MSC to release exosomes containing distinct miRNA contents, such as miR-222/223, which in turn promotes quiescence in a subset of cancer cells and confers drug resistance. Building on these results, we developed a novel, nontoxic therapeutic strategy to target dormant breast cancer cells based on systemic administration of MSC loaded with antagomiR-222/223. In an immunodeficient mouse model of dormant breast cancer, this therapy sensitized breast cancer cells to carboplatin-based therapy and increased host survival. Overall, our findings illuminate the nature of the regulatory interactions between breast cancer cells and MSCs in the evolution of tumor dormancy and resurgence in the micrometastatic microenvironment of the bone marrow. *Cancer Res; 76(19); 5832–44. ©2016 AACR.*

Introduction

Breast cancer recurrence continues to pose a major clinical problem, despite significant advancement in early diagnosis and an aggressive mode of treatment. It is widely accepted that breast cancer recurrence is linked to a prolonged dormancy and successful survival of breast cancer cells (BCC) in the bone marrow. In such state, the BCCs are in mitotic arrest and resist anticycling treatments (1–8). To prevent the recurrence of breast cancer, one potential novel approach includes targeting the dormant BCCs and/or restraining BCCs from establishing dormancy. However, because the region of dormancy is also the home of the endogenous hematopoietic stem cells in the bone marrow, this approach poses a major challenge for successful targeting of the BCCs without untoward effects on the endogenous stem cells (4, 7, 9).

Developing treatments for dormant BCCs in the bone marrow is particularly important because of similar location and noncycling phase with the hematopoietic stem cells. Therefore, for the next major advance in this area, we must first have a deeper mechanistic insight of events that allow BCCs to adapt a dormant phenotype in the bone marrow milieu. Dormant BCCs have been identified within the stromal compartment close to the endosteum (10). Bone marrow stroma establishes gap junctional intercellular communication (GJIC) with BCCs, and this partly explains how the latter survives as cycling quiescent cells in the bone marrow (11). The GJIC allows miRNAs to be exchanged between BCCs and stroma (7, 11). Interestingly, mesenchymal stem cells (MSC) can also communicate with BCCs through GJIC (12). GJIC occurs subsequent to the interaction between membrane-bound CXCR4 and CXCL12 (12, 13). Such intercellular contact creates a functional cellular chaperone that allows the MSCs to provide immune protection for the BCCs (14). In addition, MSCs can also support the survival and growth of cancer cells by their ability to differentiate into cancer-associated fibroblasts (15, 16).

Although much of our current understanding of the breast cancer dormancy is derived from interactions between BCCs and stroma (12–14), the nature of interactions between the BCCs and cells in the bone marrow microenvironment during the early phase of entry into the cavity and how BCCs adapt to cycling quiescence state remain poorly understood. MSCs are proposed to be an early source of cellular interaction with BCCs because of their anatomic location within the cavity. BCCs initially encounter MSCs after traversing the periphery into the

[1]Department of Medicine, Hematology/Oncology, New Jersey Medical School, Rutgers Biomedical and Health Sciences, Newark, New Jersey. [2]Graduate School of Biomedical Sciences, Rutgers Biomedical and Health Sciences, Newark, New Jersey. [3]H. Lee Moffitt Cancer Center and Research Institute, Tampa, Florida. [4]Department of Biochemistry and Molecular Medicine, School of Medicine and Health Sciences, George Washington University, Washington, DC. [5]Department of Pathology and Laboratory Medicine, New Jersey Medical School, Rutgers Biomedical and Health Sciences, Newark, New Jersey.

Note: Supplementary data for this article are available at Cancer Research Online (http://cancerres.aacrjournals.org/).

Corresponding Author: Pranela Rameshwar, Department of Medicine, Rutgers-New Jersey Medical School, 185 South Orange Avenue, MSB, Room E-579, Newark, NJ 07103. Phone: 973-972-0625; Fax: 973-972-8854; E-mail: rameshwa@njms.rutgers.edu

doi: 10.1158/0008-5472.CAN-16-1092

bone marrow cavity, as MSCs are anatomically located at the abluminal surface of the central vasculature (17, 18). Furthermore, even if the BCCs bypass the MSCs within the perivascular region, they can still encounter MSCs that can be located in contact with the trabeculae and/or close to the endosteum (19, 20). Thus, an understanding of how BCCs and MSCs interact during the early stages of dormancy is highly significant to develop treatment strategies.

Here, we investigated the mechanisms by which MSCs communicate with BCCs through exosomes to impart cycling quiescence. We report on BCC priming of MSCs to release exosomes with a specific profile of miRNAs. We further discovered that the miRNA contents of exosomes are responsible for conferring a cellular quiescence in a subset of BCCs. We next applied these findings to develop a therapeutic strategy to target dormant BCCs in the femurs of immunodeficient mice as a physiologically relevant experimental model. To this effect, we present evidence suggesting that MSC-loaded antago-miRNAs and reduced chemotherapy eradicated BCCs in the femurs of mice.

Materials and Methods

Cell lines

MDA-MB-231 and T47D were purchased from ATCC and cultured as per their instructions. All cell lines used in this study were tested by Genetica DNA Laboratories. Both cells were validated as the original cells using ATCC STR database (www.atcc.org.org/STR_Database.aspx).

Anti-miR-222 and -223 transfected MSCs

MSCs were cotransfected with anti-miR-223 and anti-miR-222 or negative control anti-miR using Lipofectamine RNAiMAX Reagent (Life Technologies Invitrogen). After 24 hours, the transfectants were incubated at 37°C for 30 minutes with serum-free media containing 10 μmol/L of Cell Tracker Dye CMTMR. After this, the labeled cells were washed twice with PBS.

Preparation of BCC-primed MSCs, naïve MSCs, and stimulation of BCCs

Transwell cultures were established in 6-well plates with 0.4-μm inserts. Equal amounts (6×10^4) of BCCs and MSCs were added to the outer and inner wells, respectively, in DMEM with 10% exosome-free FCS. After 24 hours, the inner wells with BCCs were discarded. The MSCs were washed with PBS and then incubated with DMEM with 2% exosome-free FCS. At 48 hours, exosomes were isolated from the MSC media. The exosomes from triplicate wells were added to duplicate naïve BCCs at 2.5×10^5 per well of 6-well plates. The BCCs were cultured in 2% exosome-free FCS. After 48 hours, the cells were analyzed for cell-cycle phase or protein.

Naïve exosomes were collected in 80% confluent MSCs cultured in 2% exosome-free FCS over a 48-hour period.

Exosome isolation

Exosomes were collected by differential centrifugation, as described previously (21), or using an Exosome Isolation Kit from Life Technologies Invitrogen. The average particle size was 96.1 nm at 1/100, resulting in about 2×10^8 particles/mL media, using the NanoSight.

Cell-cycle analyses

Cell-cycle analyses were performed as described previously (11): labeling with propidium iodide for total cycling status. G_0 and G_1 phases were discerned by colabeling with 7-aminoactinomycin D (7-AAD) and pyronin Y.

miRNA array analyses

The Human miFinder miRNA PCR Array (Qiagen) was run according to the manufacturer's instructions with RNA isolated using the miRNeasy Mini Kit. RNA (250 ng) was converted to cDNA with the miScript II reverse transcription reaction using HiSpec Buffer. The cDNA was used as templates in real-time PCR using the Human miRNome miScript miRNA PCR Array (miScript). The PCR array used the miScript SYBR Green PCR Kit. The PCR was run on the 7300 Real-Time PCR System using the following thermocycling parameters: 94°C for 15 minutes, 40 cycles at 94°C for 10 seconds, 55°C for 30 seconds, 70°C for 30 seconds, followed by a melting curve analysis.

The data discussed in this publication have been deposited in NCBI's Gene Expression Omnibus (GEO; ref. 22) and are accessible through GEO Series accession number GSE85341 (https://www.ncbi.nlm.nih.gov/geo/query/acc.cgi?acc=GSE85341). The data were analyzed with the online miScript miRNA PCR Array data analysis tool (http://www.sabiosciences.com/mirnaArrayDataAnalysis.php). To minimize the potential noise introduced by measurements below detection threshold, miRNAs with C_t value greater than 35 in all groups were considered as undetected (23–25). Specifically, the expression levels of miRNAs were evaluated by a comparative C_t method using global median of expressed miRNA on the plate for normalization. The data were only used if the output passed the quality control test with respect to array reproducibility and reverse transcriptase efficiency.

In vivo studies

Female nude BALB/c mice (6 weeks) were obtained from Charles River Laboratories and then housed in an AALAC-accredited facility at Rutgers, New Jersey Medical School (Newark, NJ). The protocol was approved by the Institutional Animal Care and Use Committee, Rutgers School of Biomedical Health Sciences (Newark, NJ).

The method to establish breast cancer dormancy was described previously (7). Briefly, 10^3 of freshly sorted $Oct4^{hi}$ BCCs (MDA-MB-231 or T47D) in 0.2 mL PBS were injected in the tail veins of mice. The $Oct4^{hi}$ BCCs have been shown to have cancer stem cell functions (7). At days 2 and 4, the mice were injected intraperitoneally with low dose of carboplatin (2.5 mg/kg). At day 3, the $Oct4^{hi}$ BCCs were located within the endosteal regions of femurs (7). At day 6, the mice were injected intravenously with 10^6 MSCs, transfected with anti-miR-222/223 or control anti-miRNA. The MSCs were also labeled with the tracker dye CMTMR. At days 9 and 11, the mice were injected with 5 mg/kg carboplatin i.p. At day 18, the mice were euthanized and the femurs analyzed for the following: real-time PCR for human PPIB; microscopic examination for fluorescence cells on tissues scraped from the endosteal region; and IHC for cytokeratin with paraffin-embedded decalcified femurs. Analyses with several housekeeping genes identified PPIB as the most sensitive and consistent with regards to the detection of human cells in mouse. Survival studies were done for 8 weeks with 8 mice.

Dormancy was established with BCCs, stably transfected with pEGFP1-Oct3/4 and Cx43 shRNA, as above. Seventy-two hours later, the mice were injected intraperitoneally with 100 mg/kg AMD3100 and carboplatin using the same schedule as above. After treatment, the mice were euthanized and the femurs removed for analyses described below.

Statistical analysis

Statistical data analyses were performed with ANOVA and Tukey–Kramer multiple comparisons test. $P < 0.05$ was considered significant.

Results

Exosome transfer between MSCs and BCCs

We first characterized the MSC-derived exosomes by transmission electron microscopy and Western blotting for two tetraspanin proteins, CD63 and CD81 (Fig. 1A and B). The presence of the tetraspanins supported an endosomal origin of the secreted vesicles, consistent for exosomal nature of these vesicles (26, 27). We next validated the transfer of exosomes between MSCs and BCCs in a Transwell system separated by 0.4-μm membranes (Fig. 1C). BCCs and MSCs, stably transfected with pCD63-GFP, released green fluorescence exosomes, indicating that the analytic system used here could track exosome transfer (Fig. 1D and E and Supplementary Fig. S1B and S1C). The pCD63-GFP transfectants were designated as "donors" and the untransfected cells, "Receivers." At 24 and 48 hours postculture, the released vesicles showed a sharp peak of mostly 98 nm vesicles, thereby eliminating the release of apoptotic bodies, which range at 500 to 5,000 nm (Fig. 1F; Supplementary Movie 1; ref. 26). Flow cytometry of receiving cells cultured for 48 hours showed a right shift (red), validating successful transfer of exosomes from the donor cells (Fig. 1G). A corollary study with the donor cells in the lower chamber resulted in overlap with vector transfectant, indicating little transfer of exosomes against gravity (Fig. 1G). However, confocal images of Z-sections showed some upward transfer of the exosomes (Fig. 1H; Supplementary Movies 2 and 3). These results suggest that exosomes can be transferred against gravity, although at significantly reduced efficiency.

Cycling effects of naïve MSC-derived exosomes on BCCs

To study how MSC-derived exosomes affect the cycling effects of BCCs (7, 13, 28), we transferred exosomes from naïve MSCs (never exposed to BCCs) and then added them to fresh BCCs. After 48 hours, Western blots showed increases in cyclin D1 and CDK5 for MDA-MB-231 cells but no change in T47D cells (Fig. 2A and Supplementary Fig. S2). Propidium iodide labeling indicated that the naïve exosomes promoted the ratio of the S-phase for MDA-MB-231 cells and G_2 phase for T47D cells (Fig. 2B). Further analyses, based on the DNA and RNA contents, indicated that the exosomes transitioned a subset of BCCs into cycling quiescence (Fig. 2C). T47D cells showed a small population in the G_0 phase, based on low to undetectable RNA (red arrow) and another subset with relatively higher RNA content (G_1 phase). Together, these findings suggested that exosomes from naïve MSCs enhanced a population of BCCs into cycling phase and a relatively smaller subset in the G_0–G_1 phase.

Cycling effects by exosomes from breast cancer–primed MSCs

We next asked whether exposure to BCCs can change the cycling effects of the MSC-derived exosomes (primed exosomes). We primed MSCs in a Transwell system as outlined in Fig. 3A. The exosomes from primed MSCs were added to fresh BCCs for cell-cycle analyses. Propidium iodide labeling showed similarities between naïve and primed exosomes (Fig. 3B). Further analyses of the DNA and RNA contents revealed that the primed exosomes caused a significant ($P < 0.05$) increase in low DNA in a subset of MDA-MB-231 cells (Fig. 3C). The population with low DNA was in G_0 phase (low pyronin-Y), increasing from 0.75% at baseline (no exosome) to 2.5% for naïve exosomes, then to 3.2% for primed exosomes (Fig. 3C). The effects of the primed exosomes seemed to be cell-specific, as there was no marked difference for the less evasive and metastatic T47D cells (Fig. 3C). Western blot analyses of extracts from BCCs treated with primed exosomes showed decreases in CDK4, cyclin D1, and p21WAF1 (Fig. 3D and Supplementary Fig. S3). Increased CDK6 was expected for the highly proliferating MDA-MB-231 cells, as the subset of cells in the G_0 phase was relatively small (Fig. 3C). Together, primed exosomes were more effective in changing the cycling status of a subset of MDA-MB-231 cells, but such difference was not seen in T47D cells.

miRNA-containing exosomes support cycling changes in BCCs

We investigated the possibility that the miRNA contents of exosomes were responsible for the noted cycling changes in BCCs. To address this, we collected exosomes from primed MSCs in which the pre-miRNAs could not mature. These studies were conducted with MSCs knocking down the endogenous dicer (Supplementary Fig. S4A). We found that the exosomes from these MSCs failed to impart cycling quiescence; instead, they caused the majority of MDA-MB-231 cells to transition into the S-phase, relative to control siRNA (Fig. 4A and Supplementary Fig. S4B). These studies revealed an inherent role for miRNAs in the observed effect of exosomes in cycling quiescence of BCCs. Although pri-miRNA is nuclear, we nonetheless assess its level in the exosomes. Primers specific for pri-miR-222 showed C_t values above the maximum threshold for exosomal RNA, whereas similar evaluation in the source MSCs resulted in C_t of 26 ± 0.03.

A heatmap of miRNAs from exosomes of naïve and primed MSCs illustrated distinct miRNA profiles (Fig. 4B). Scatter plots with the boundaries set at ± 1.5 fold changes indicated similarities as well as distinct differences between two groups (Fig. 4C and D). Ingenuity pathway analyses of T47D-primed/naïve MSCs demonstrated a network with genes linked to the G_1/S-phase and tumor proliferation (Supplementary Fig. S5A). Similarly, MDA-MB-231 cell–primed exosomes narrowed miRNAs involved in the expression of cell-cycle genes (Supplementary Fig. S5B). Overall, the predictive analyses were consistent with the functional studies, showing a subset of BCCs transitioning into cycling quiescence by exosomes from breast cancer–primed MSCs (Fig. 3).

Reverse dormancy by targeted miR-222/223

We selected miR-222 and -223 as potential targets to reverse the cycling quiescence of BCCs for drug sensitivity, based on the following reasoning: their roles in BCC quiescence in bone marrow, increased levels in MSCs and MSC-derived exosomes, increases by 3- to 5-fold in primed relative to naïve exosomes, and the link of miR-222 to tumor resistance (Figs. 4B and 5A–C and Supplementary Fig. S6A and S6B; refs. 11, 29). Thus, miR-222/223 could have a role in early development of cycling quiescence, leading to dormancy. Thus, we targeted these miRNAs by delivering the respective antagomiRs within MSCs *in vivo* (30–32). We first tested whether

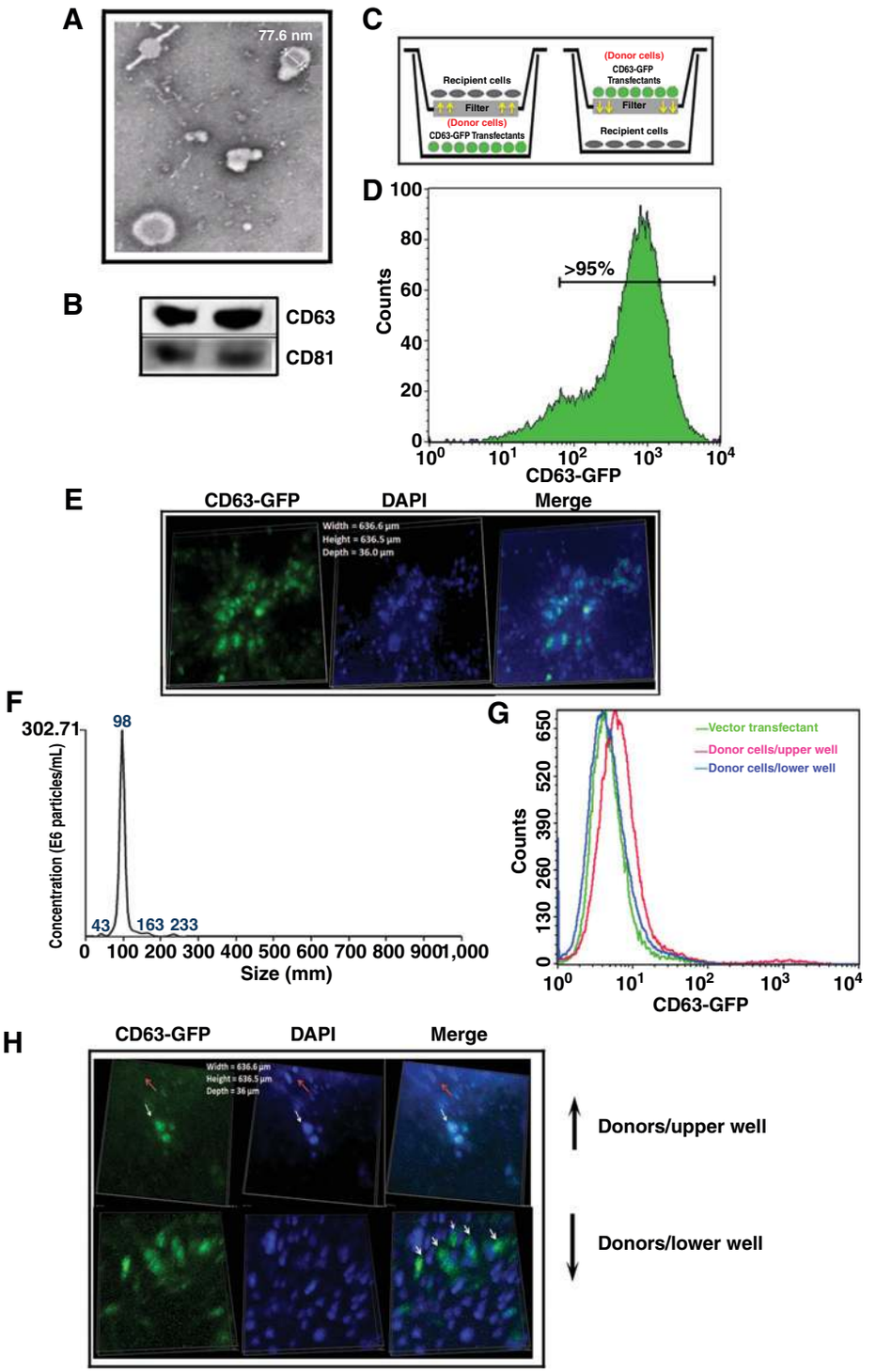

Figure 1.
Characterization and intercellular transfer of exosomes. **A,** representative TEM images of MSC-derived exosomes. **B,** Western blot analysis for CD63 and CD81 with extracts from MSC-derived exosomes from two different donors. **C,** a Transwell system with donor cells, stably transfected with pCD63-GFP, and untransfected receiving cells. **D,** flow cytometry for GFP with MDA-MB-231 cells, stably transfected with pCD63-GFP. **E,** representative 3-dimensional image of pCD63-GFP-MDA-MB-231, merged with DAPI images. **F,** representative histogram of nanoparticle tracking analysis with media from the Transwell cultures in **C**. **G,** flow cytometry for GFP in the recipient cells in 48-hour Transwell cultures from **C**. **H,** confocal microscopy of >10 fields in **C**. Top, recipient cells were placed in the upper wells; bottom, recipient cells in the lower wells; white arrows, GFP^+ cells; red arrows, GFP^- cells.

the anti-miRNA can be released from MSCs in a Transwell system. Flow cytometry indicated efficient transfer of cyanine 5 (Cy5)-tagged anti-miR-222 to approximately 78% BCCs after 48 hours (Fig. 5D). Because the MSCs remained viable and did not migrate through the membrane, we concluded that the observed transfer of miRNAs was through microvesicles.

The function of the transferred anti-miRNA was assessed in drug sensitivity analyses (29, 33). Primed MSCs were transfected with Cy5-anti-miR-222 or Cy5-control anti-miR. Exosomes from these MSCs were transferred to fresh BCCs for assessment of total and active P-glycoprotein (P-gp). Using specific antibodies (34), flow cytometry analyses (Fig. 5E) indicated an increase in total P-gp

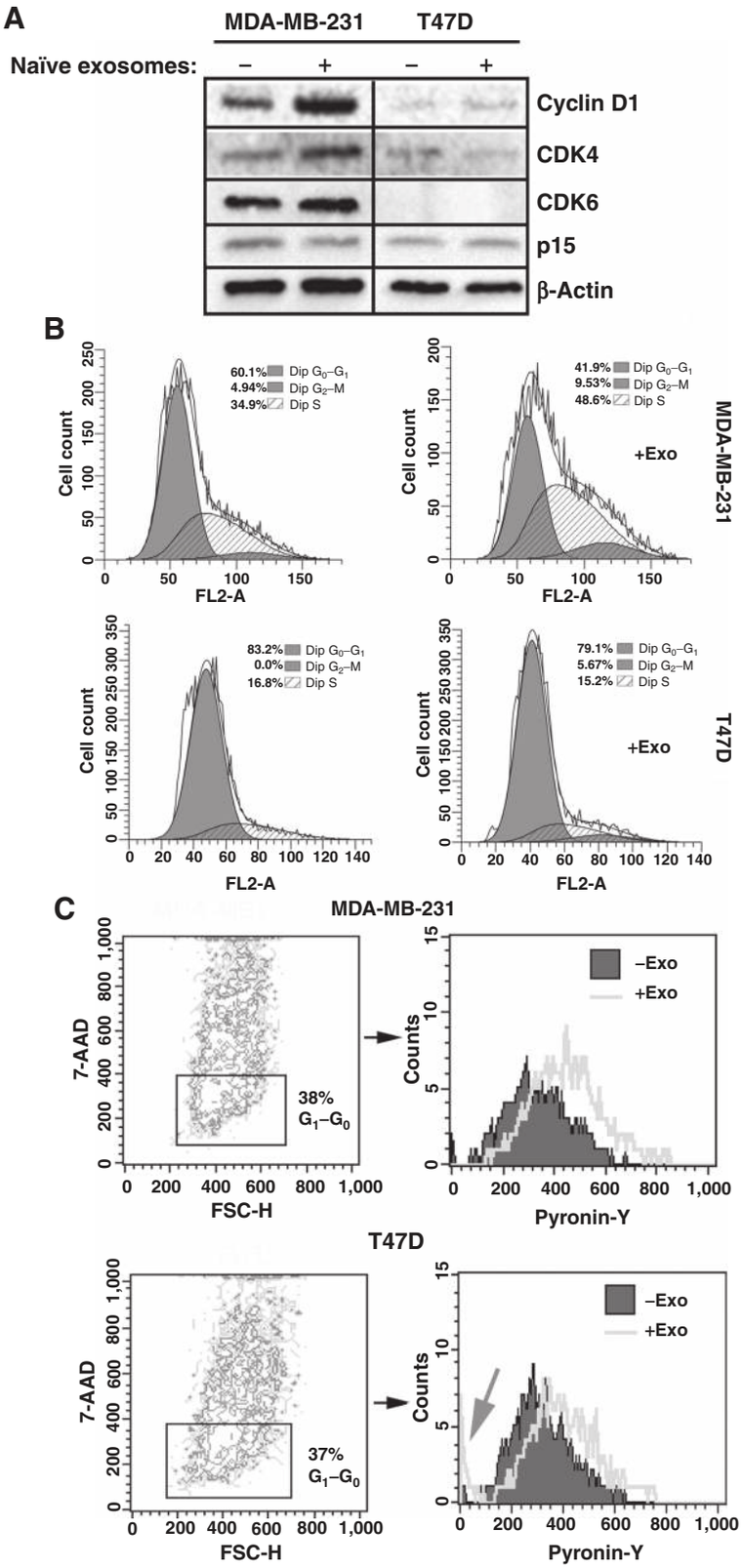

Figure 2.
Cell-cycle analyses in BCCs treated with exosomes from naïve MSC. **A,** BCCs untreated or treated with exosomes (+exo) from naïve MSCs. After 48 hours, whole-cell extracts were analyzed by Western blot analysis for cyclin-associated proteins and normalized for β-actin. **B,** BCCs were treated as in **A** and then studied for cell-cycle analyses by propidium iodide. The figure represents three experiments with exosomes collected different MSC donors. **C,** the studies in **B** were repeated, except for colabeling with 7-AAD and pyronin-Y. The low DNA content (boxed region, left) was stratified for pyronin-Y incorporation (right). The figure represents three experiments with exosomes from different MSC donors.

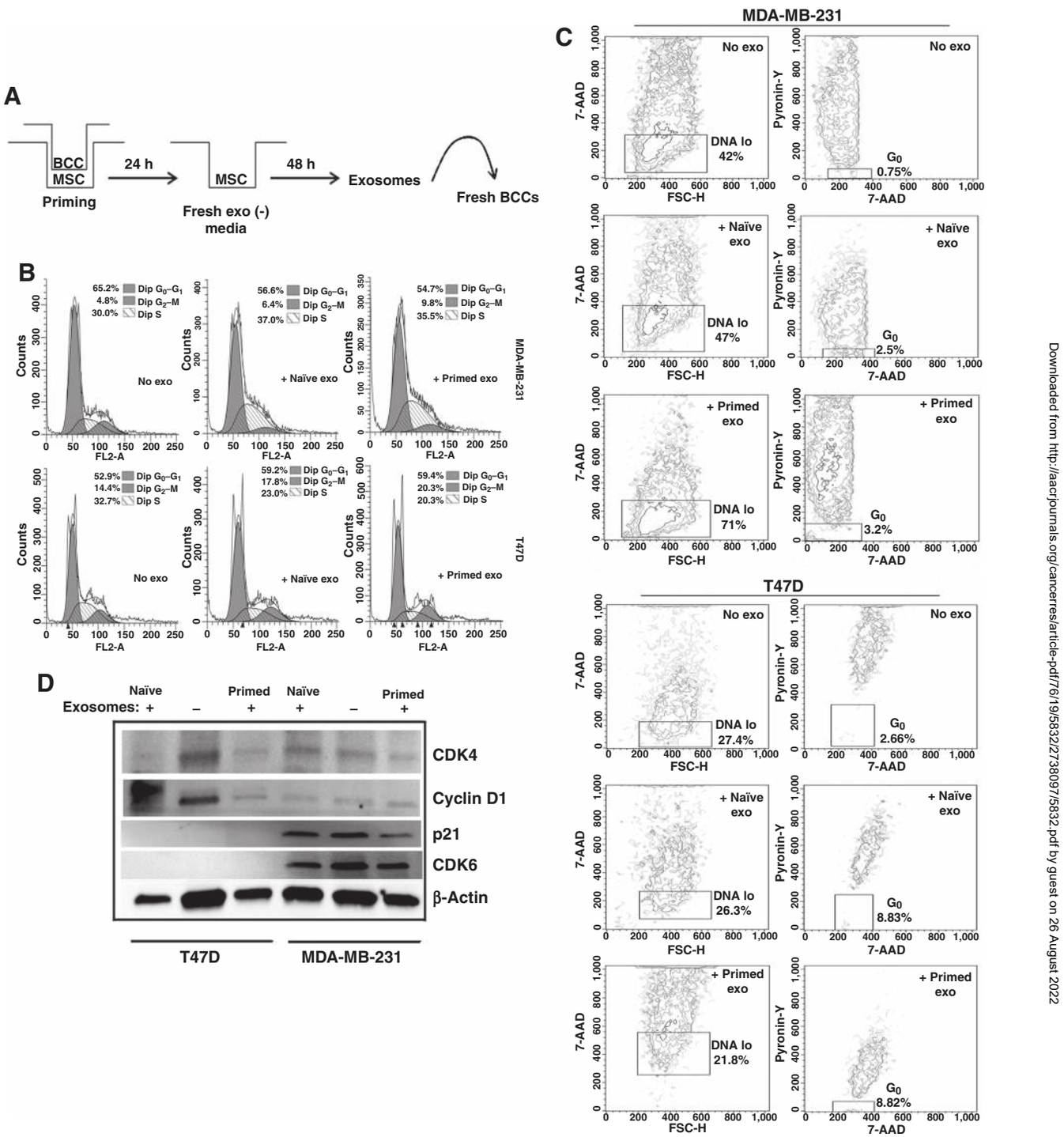

Figure 3.

Cell-cycle analyses of BCCs treated with naïve and primed exosomes. **A,** shown is the method to prime MSCs with BCCs. The cells were separated by 0.2-μm membranes in exosome-free media. After 24 hours, the inner well was discarded and the medium replaced. Exosomes were collected in the media after 48 hours for addition to fresh BCCs. **B,** at 48 hours, BCCs treated with primed and naïve exosomes were analyzed for cell cycle by propidium iodide. **C,** the studies in **B** were repeated with 7-AAD and pyronin Y labeling. **D,** representative of three experiments in which whole-cell extracts from the cells in **B** were analyzed by Western blot analysis for cyclin-associated proteins and β-actin.

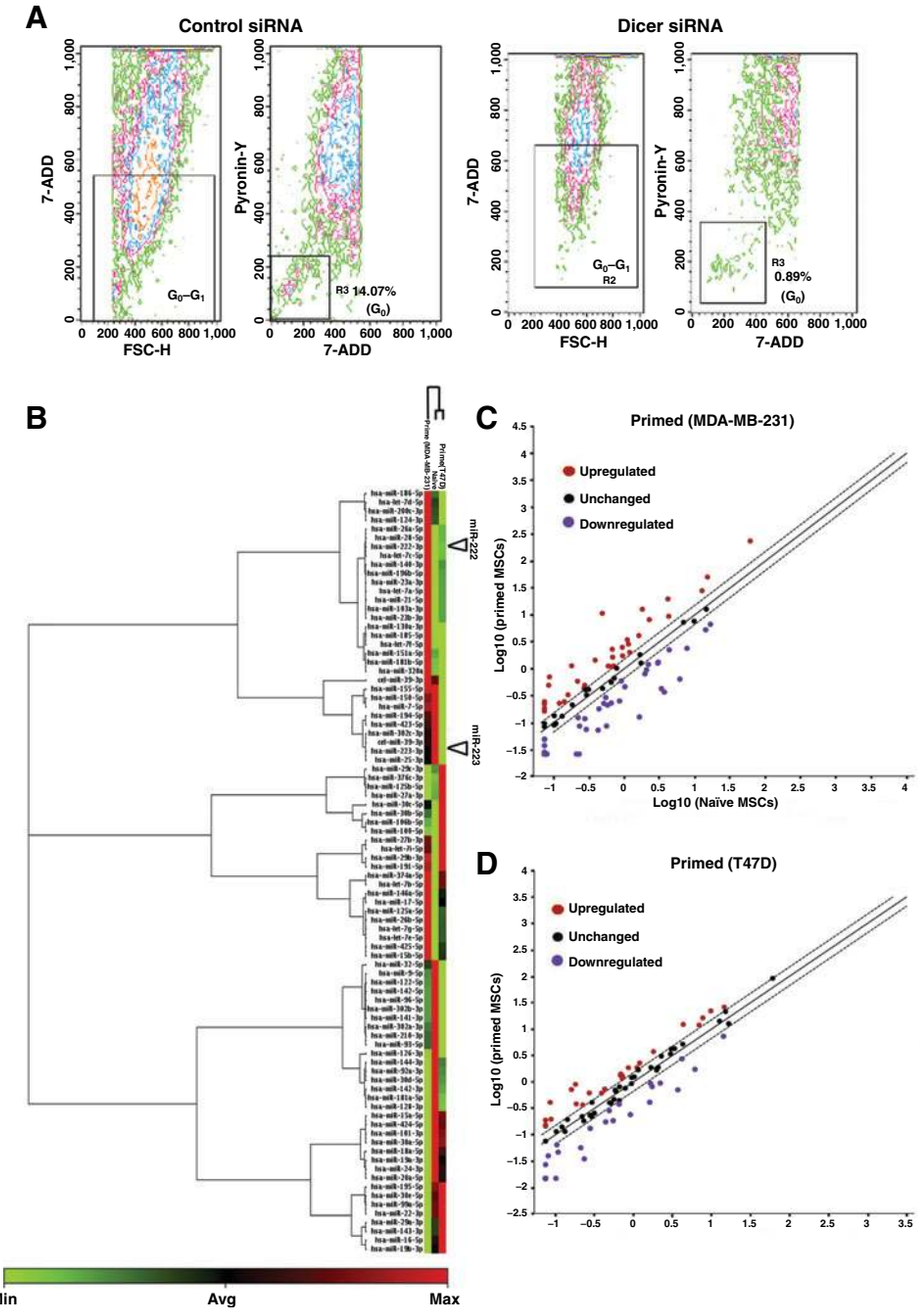

Figure 4.
Cell cycle with exosomes from dicer knockdown MSCs; miRNA array analyses with exosomes from naïve and breast cancer–primed MSCs. **A,** exosomes from dicer- or control siRNA–transfected MSCs were added to BCCs for cycling analyses with 7-AAD and pyronin Y. **B,** a cluster map is shown for the output of miRNA arrays from naïve and primed exosomes. **C** and **D,** scatter plots with cutoffs at 1.5-fold are shown for miRNAs within exosomes of primed/naïve MSCs.

(left) and reduced in the active form (right). These findings were consistent with dye efflux studies, which showed a significant ($P < 0.05$) retention of calcein by anti-miR-222–containing exosomes, relative to control anti-miRNA (Fig. 5F). Together, these findings indicated that anti-miR-222 influences the activity of a drug transporter in the BCCs to favor drug sensitivity.

A therapeutic efficacy of anti-miR-222/223

We next developed a treatment strategy for dormant BCCs with anti-miR-222/223 and a lower dose of carboplatin in an *in vivo* model of breast cancer dormancy (Fig. 6A). Mice were injected with CMTMR (orange/red)-labeled MSCs and transfected with anti-miR-222/223 or control anti-miRNA. After 48 hours, the mice were injected intraperitoneally with reduced (<4×, 2.5 mg/kg) carboplatin or vehicle in 0.5 mL, twice at 2-day intervals (7, 13). After one week, the femurs were flushed and then examined for human cells. We expected few to undetectable dormant BCCs in the endosteal region (7). Technical control for murine GAPDH indicated C_t values of approximately 20 (Fig. 6B). Primers for human PPIB (cyclophilin B) detected ≥5 BCCs/10^6 murine cells (Supplementary Fig. S7). Human cells were undetectable in the anti-miRNA/carboplatin-treated mice ($C_t > 40$), as compared with C_t values of approximately 25 for mice given control anti-miRNA (Fig. 6B).

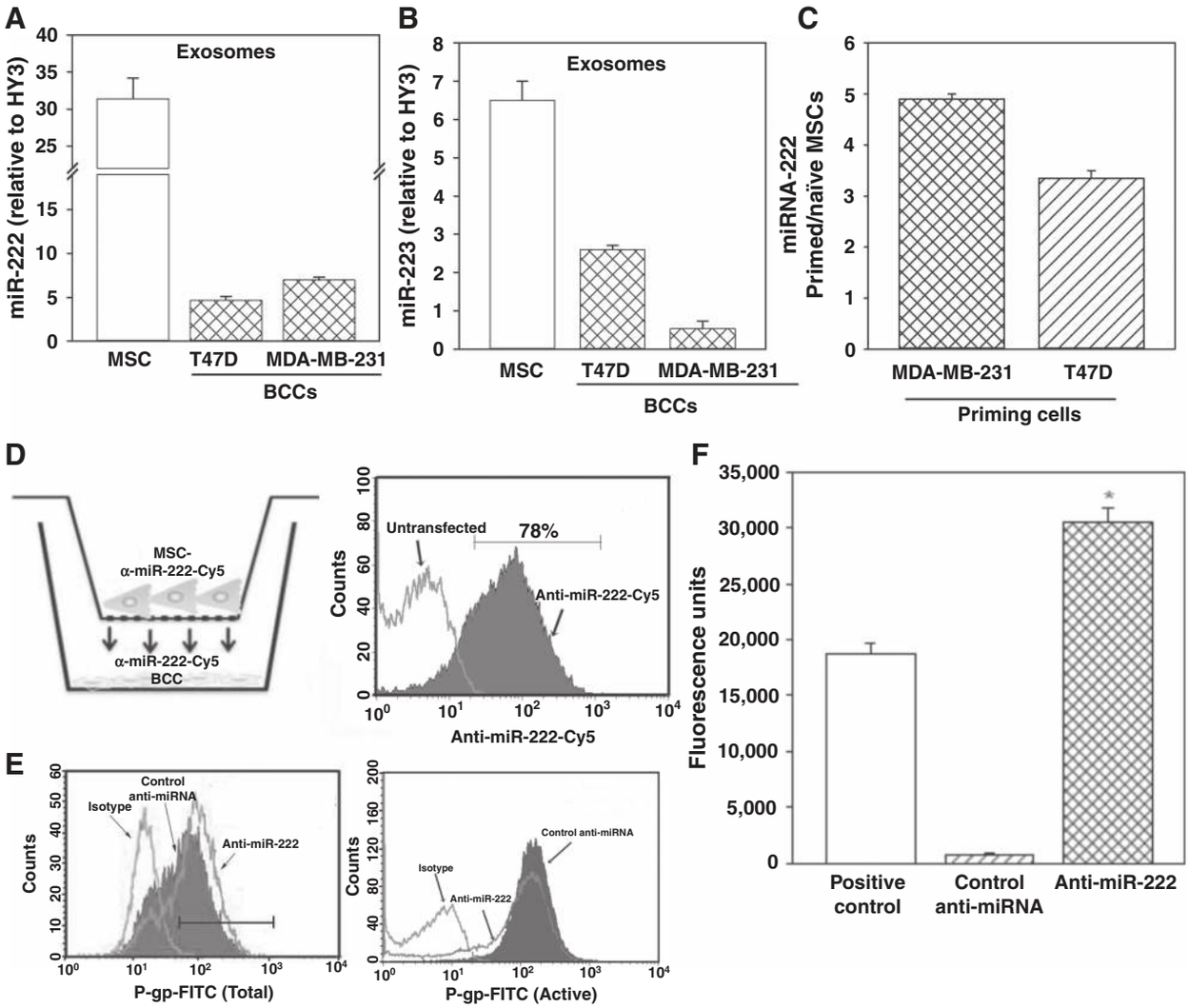

Figure 5.

miR-222/223 in cell-cycle quiescence and drug resistance. **A** and **B,** real-time PCR for miR-222/223 with RNA from naïve exosomes. The results are presented relative to HY3, mean ± SD, $n = 4$. **C,** the level of miR-222 is presented as primed/naïve exosomes, mean ± SD, $n = 4$. **D,** left, cocultures were established with MSCs, transfected with Cy5-tagged anti-miR222 (anti-miR-222-Cy5) in the upper wells, and the recipient untransfected MDA-MB-231 or T47D cells in the lower wells; right, after 48 hours, the BCCs were analyzed for Cy5 by flow cytometry; representative figure is shown for MDA-MB-231 cells. MSCs were transfected with anti-miR-222 or control anti-miRNA and then primed with MDA-MB-231 cells. Exosomes were collected from the primed MSCs and then added to fresh MDA-MB-231 cells. **E,** after 48 hours, the BCCs were analyzed by flow cytometry for total and active P-gp with specific antibodies. The studies in **E** were repeated; instead, the MDA-MB-231 cells were studied for calcein efflux. Positive control contained verapamil. **F,** data are presented as the mean fluorescence of retained dye ± SD, $n = 5$. *, $P < 0.05$ versus control anti-miRNA.

As the injected dormant BCCs were transfected with Oct4^{hi}-GFP (7), we examined the endosteal region for green fluorescent cells. Such cells were found in mice given control anti-miRNA and carboplatin (Fig. 6C, arrows, top/left). In contrast, mice given anti-miR-222/223 and carboplatin were devoid of green cells (Fig. 6C, top/right). As human cells were not detected in the femurs of mice given anti-miR-222/223/carboplatin (Fig. 6B), we asked whether the carboplatin killed the injected MSCs. A dose–response *in vitro* study with carboplatin and MSCs indicated survival at <50 μg/mL carboplatin (Supplementary Fig. S8). An examination of cells scraped from the endosteal region of the femurs identified clusters of CMTMR^{+} cells in mice with control anti-miRNA as compared with few orange cells for anti-miR-222/223 and carboplatin treatment (Fig. 6C, bottom). The findings indicated that the MSCs migrate toward the dormant BCCs in the endosteum. Those loaded with antagomiRs became sensitive to carboplatin.

After establishing that anti-miR-222/223 facilitated chemosensitivity in the dormant BCCs, we investigated whether this effect can be explained by increased cellular proliferation. Sections of the decalcified femurs, labeled with anti-Ki67, identified a large number of positive cells in the endosteum of mice with antagomiRs as compared with undetectable Ki67 cells given control anti-miRNA (Fig. 6D, arrows). In addition, we confirmed that the

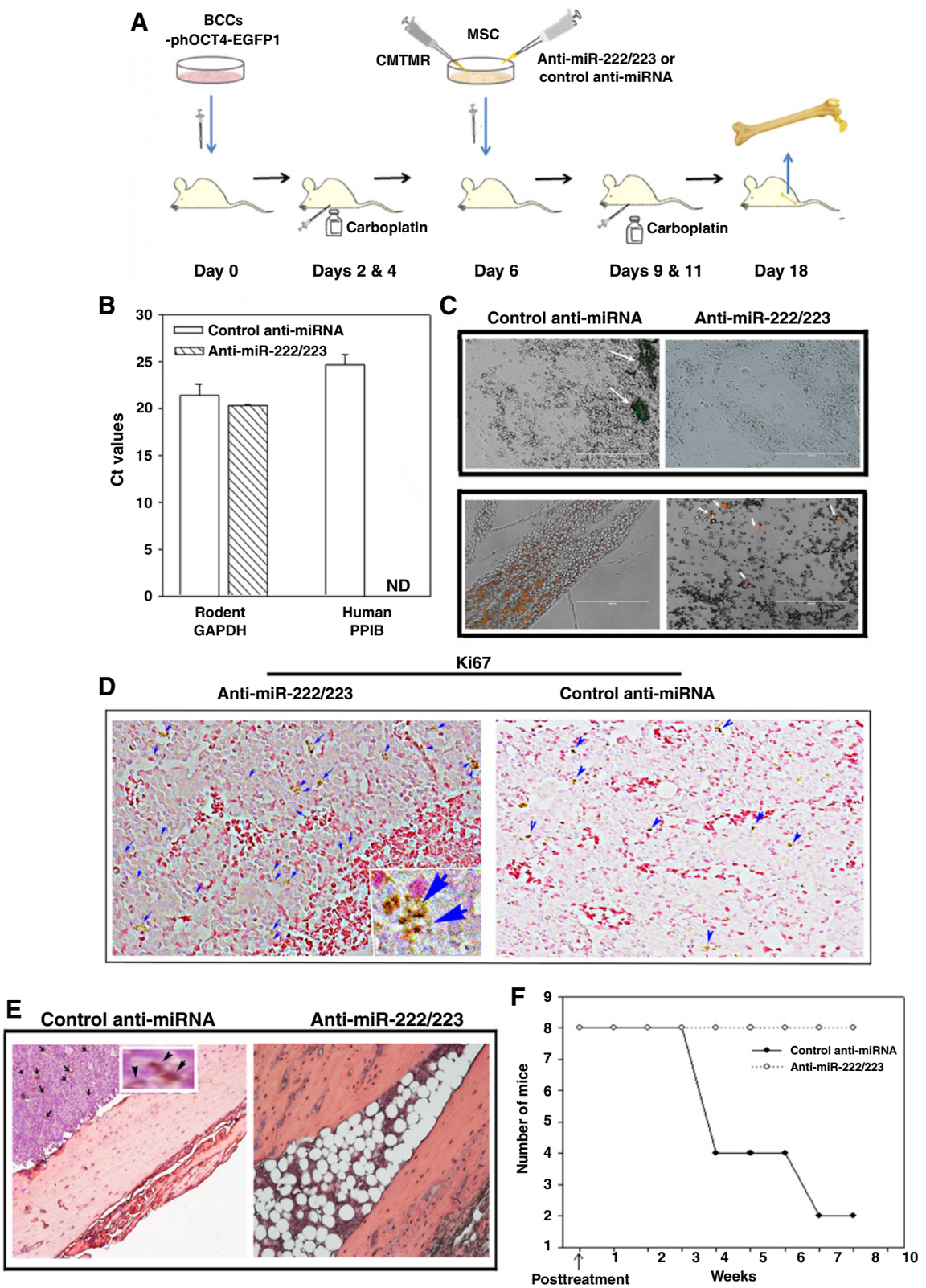

BCCs were targeted by labeling with a pan-cytokeratin antibody (brown spots). We observed several brown spots in mice with control anti-miRNA (arrows) with few spots for mice treated with anti-miR-222/223 (Fig. 6E).

To determine whether the dual treatment improved the survival of the recipient mice, we monitored the mice ($n = 8$/group) for 2 months. Carboplatin and anti-miR-222/223 treatment resulted in total survival during the observational period. However, mice treated with carboplatin and control anti-miRNA succumbed at about week 3 (Fig. 6F, solid line). Taken together, these results showed an efficient delivery of anti-miR-222/223 by bone marrow–derived MSCs to femurs and that antagomiRs improved the efficiency of carboplatin by requiring a lower dose to target the BCCs.

Therapeutic delivery of antagomiR

Anti-miRNAs can be transferred from MSCs to BCCs through exosomes and GJIC (11, 12, 32). We experimentally tested the possibility that MSCs could deliver anti-miR-222/223 to the dormant BCCs through GJIC-dependent and independent methods using the strategy outlined in Fig. 7A. Dormancy was established with $Oct4^{hi}$ (green) BCCs, previously shown to be cancer stem cells, or with similar BCCs knocked down for Cx43 (shRNA/red). This allowed for studies in which GJIC between MSCs and BCCs can be formed or blunted (7). The mice were injected intravenously with MSCs transfected with anti-miR-222/223 or control anti-miRNA. In the absence of GJIC, CXCL12 can be increased to enhance the proliferation of BCCs (11, 35) Thus, to maintain cycling quiescence of the CX43 knockdown BCCs, we preserved low activity of CXCL12 by treating with vehicle or AMD3100. Also, AMD3100 prevented BCCs from interacting with MSCs through membrane CXCL12 and CXCR4 (13).

The close location between the dormant BCCs (green) and Far Red–labeled MSCs was indicated by yellow fluorescence (Fig. 7B, inset in the top left panel). One week after treatment, yellow cells ($Oct4^{hi}$ with Cx43 shRNA) were markedly reduced by anti-miR-222/223/carboplatin/AMD3100 treatment (Fig. 7B, bottom right). The remaining red/green cells suggested that the antagomiRs may also require GJIC for transfer to the BCCs. These findings were also independently validated when the decalcified femurs were labeled for cytokeratin (Fig. 7C). The arrows showed the alkaline phosphatase (brown)–positive BCCs. In brief, we found that MSCs also release anti-miR-223/-222 to the surrounding BCCs. In addition, the observed transfer of anti-miRNAs could occur through both GJIC-dependent or -independent manner.

Discussion

Findings presented here reveal how MSCs initiate a quiescent phenotype in BCCs and opened up a new avenue to target miRNA within stem cells for therapeutic gains. We also found that MSCs can be effectively used as a cellular delivery system for antagomiRs to enhance the therapeutic efficacy of chemotherapy. These findings are particularly relevant to targeting dormant BCCs in the bone marrow, which can survive for more than a decade. We provide evidence to demonstrate how BCCs instruct MSCs to release exosomes with distinct miRNAs, resulting in cycling quiescence of a subset of BCCs. These findings are different from other reports that showed breast cancer–derived exosomes preparing metastatic sites (36). The analyses for the cell cycle–linked genes, although seemed inconsistent, can be reconciled because the effects of the exosomes occurred in a relatively small subset of BCC (Figs. 2A and 3D). Although miR-222/223 were able to reverse the proliferation of the dormant BCCs (Fig. 6D), it is unclear whether these miRNAs are targets for the cyclins. Hence, our findings highlight the need to further identify the nature of such subsets of BCCs and to dissect how distinct subsets communicate with MSCs (7, 37, 38).

The Transwell model recapitulated early communication between MSCs and BCCs entering the bone marrow and allowed us to study noncontact interactions between MSCs and BCCs (12, 17). The overall findings on miRNAs, including the distinct profiles within exosomes from naïve and breast cancer–primed MSCs suggested that the BCCs might influence the MSCs to favor their survival (Fig. 4). The results further support a key role for the miRNA content of exosomes in the cycling phase of BCCs (Supplementary Figs. S4 and S5). Both naïve and primed exosomes exerted cycling quiescence in MDA-MB-231, but there was an increase with primed exosomes (Fig. 2). This supported a role for MSCs in the immediate response to facilitate BCC survival. Future studies to dissect the BCC subsets are needed to understand how MSCs might change the heterogeneity of BCCs for drug evasion.

miR-222/223, shown to be involved in GJIC between BCCs and bone marrow stroma, were increased in the primed exosomes (11). *In vivo* targeting of these miRNAs reversed the quiescent phase of BCCs, into chemosensitive cells (Figs. 6 and 7). More importantly, anti-miR-222/223 permitted us to use four times less carboplatin, with the mice surviving during the observational period (Figs. 6 and 7). The *in vitro* studies provided a possible explanation for the positive *in vivo* outcome with the anti-miRNAs. Indeed, anti-miR-222 was able to retain calcein in BCCs and decreased the expression of active P-gp, indicating drug sensitivity (Fig. 5).

In vivo studies presented here provide several major insights: First, the MSCs were effective in homing to the bone marrow, suggesting a memory of MSCs to home to their source organ; second, the effect of antagomiR-loaded MSCs was specific to the release of the anti-miRNA rather than other endogenous factors because control anti-miRNA could not elicit a therapeutic effect (Fig. 6); thirdly, the antagomiRs increased the sensitivity of the injected MSCs to carboplatin, suggesting a therapeutic strategy to eliminate injected MSCs after their use in drug delivery.

Figure 6.
Therapeutic delivery of anti-miRNA. **A,** scheme for *in vivo* treatment of dormant BCCs. The MSCs with CMTMR (red) label were transfected anti-miR-222/223. **B,** real-time PCR for rodent GAPDH and human PPIB with total RNA from cells, flushed from the femurs of mice given control anti-miR or anti-miR-222/223. The results are presented as the mean C_t values ± SD, $n = 6$. ND, not detected ($C_t > 40$). **C,** cells scraped from the femurs of mice given control anti-miR or anti-miR-222/223 and carboplatin were examined under the EVOS FL fluorescence imager. Arrows, presence of GFP cells; organ cells, CMTMR-labeled MSCs. **D,** sections of decalcified femurs from **C** were labeled with anti-Ki67 and then counterstained with eosin. Arrows, $Ki67^+$ cells. **E,** sections of decalcified femurs of mice given control anti-miRNA or anti-miR-222/223 were labeled for human NuMA (brown) and then counterstained with Harris modified hematoxylin. Arrows, $NuMA^+$ cells. **F,** survival of mice ($n = 8$) was followed after the last treatment with carboplatin and control miRNA or anti-miR-222/223.

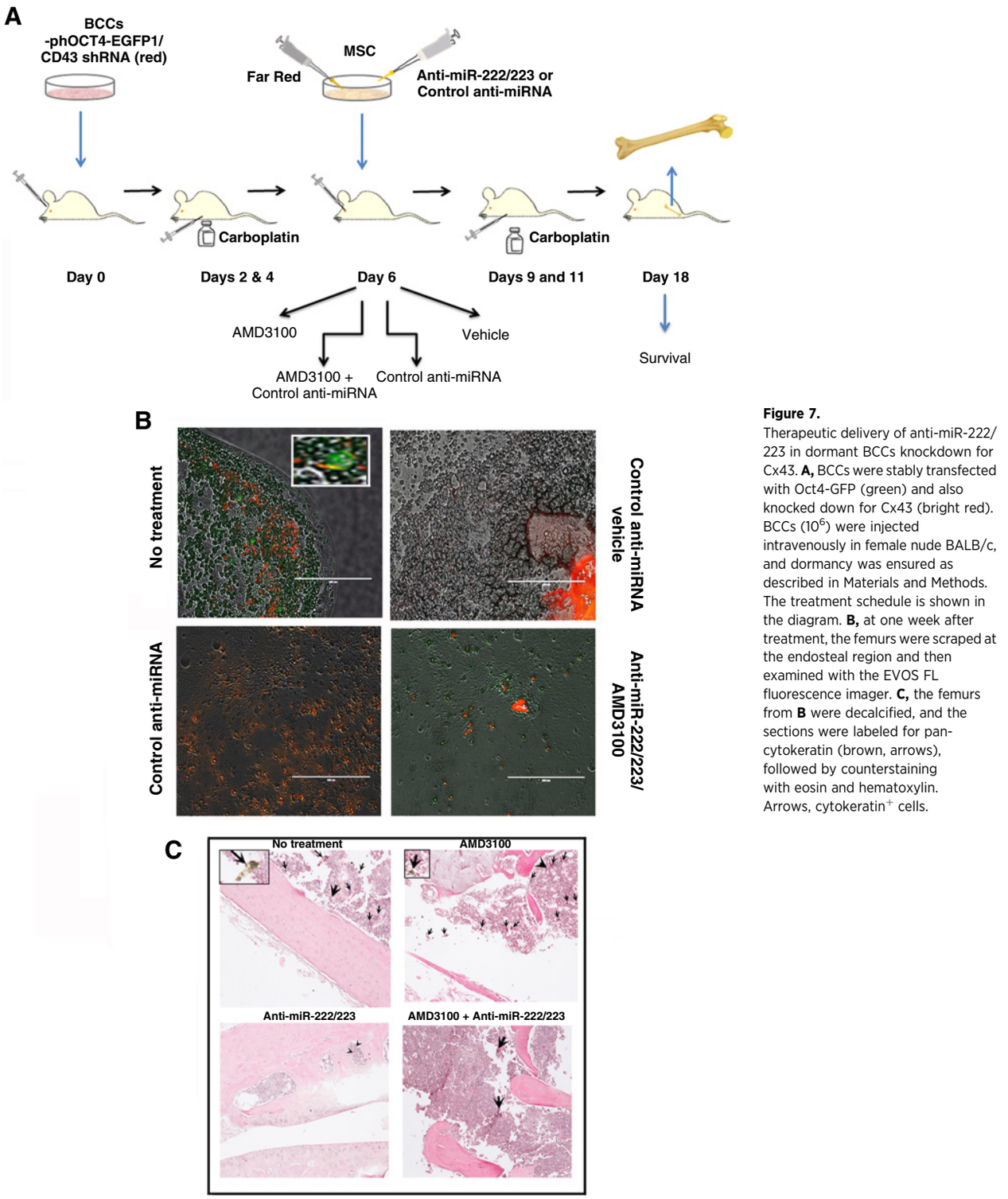

Figure 7.
Therapeutic delivery of anti-miR-222/223 in dormant BCCs knockdown for Cx43. **A,** BCCs were stably transfected with Oct4-GFP (green) and also knocked down for Cx43 (bright red). BCCs (10^6) were injected intravenously in female nude BALB/c, and dormancy was ensured as described in Materials and Methods. The treatment schedule is shown in the diagram. **B,** at one week after treatment, the femurs were scraped at the endosteal region and then examined with the EVOS FL fluorescence imager. **C,** the femurs from **B** were decalcified, and the sections were labeled for pan-cytokeratin (brown, arrows), followed by counterstaining with eosin and hematoxylin. Arrows, cytokeratin$^+$ cells.

Studies in which Cx43 was knocked down indicated that the "cargo" MSCs can transfer the antagomiRs to BCCs by GJIC and, in this case, to a lesser extent, by a GJIC-independent method (Fig. 7). Cx43 has been shown to be required for GJIC between MSCs and BCCs (12). These findings indicated that we might be able to use the described approach to treat all BCC subsets.

The findings presented here further enhance our understanding of how BCCs influence MSCs to release exosomes with distinct miRNAs. The BCCs could be instructing MSCs through soluble

factors, such as cytokines as well as exosomes. Studies on such two-way communication also explain how BCCs use bone marrow microenvironmental cells for their survival. As the bone marrow is also the site of hematopoiesis, studies are needed to determine the possible toxicity of such a treatment strategy to the hematopoietic system.

This study adds to the complex path toward breast cancer dormancy. The findings complement results from other studies showing how MSCs protect BCCs from the immune response (14). The findings also show how BCCs, other than the cancer stem cells, might be aided by MSCs to exit dormancy (7, 39). In summary, these findings show BCCs priming MSCs to produce exosomes with distinct miRNA profiles. The exosomes enter BCCs to initiate cycling quiescence. The miRNAs can be targeted using MSCs to deliver antagomiRs to chemosensitize the BCCs and to prevent dormancy. The promising use of antagomiRs in combination with a reduced carboplatin dose was not toxic because the mice survived. Our therapeutic approach is consistent with the position taken by the International Society of Microvesicles on exosomes as focal consideration for the development of treatments (40).

Disclosure of Potential Conflicts of Interest

No potential conflicts of interest were disclosed.

Authors' Contributions

Conception and design: S.A. Bliss, R. Kumar, P. Rameshwar
Development of methodology: S.A. Bliss, G. Sinha, O.A. Sandiford, S.J. Greco, M. Bryan
Acquisition of data (provided animals, acquired and managed patients, provided facilities, etc.): S.A. Bliss, G. Sinha, O.A. Sandiford, L.M. Williams, D.J. Engelberth, K. Guiro, L.L. Isenalumhe, M. Bryan, P. Rameshwar
Analysis and interpretation of data (e.g., statistical analysis, biostatistics, computational analysis): S.A. Bliss, D.J. Engelberth, K. Guiro, L.L. Isenalumhe, N.M. Ponzio, P. Rameshwar
Writing, review, and/or revision of the manuscript: S.A. Bliss, G. Sinha, O.A. Sandiford, L.M. Williams, D.J. Engelberth, K. Guiro, S. Ayer, R. Kumar, N.M. Ponzio, P. Rameshwar
Administrative, technical, or material support (i.e., reporting or organizing data, constructing databases): L.M. Williams, S. Ayer, N.M. Ponzio, P. Rameshwar
Study supervision: N.M. Ponzio, P. Rameshwar

Acknowledgments

We thank Luke Fritzky and Joel Pierre from the Digital Imaging and Histology Core facility at New Jersey Medical School for assisting with the processing of mouse femurs. We also thank Raj Patel for his assistance with the TEM study of the exosomes.

Grant Support

The work was supported by an award given by the Department of Defense (W81XWH-11-1-0276 to P. Rameshwar).

The costs of publication of this article were defrayed in part by the payment of page charges. This article must therefore be hereby marked *advertisement* in accordance with 18 U.S.C. Section 1734 solely to indicate this fact.

Received April 21, 2016; revised July 8, 2016; accepted July 27, 2016; published OnlineFirst August 28, 2016.

References

1. Habeck M. Bone-marrow analysis predicts breast-cancer recurrence. Mol Med Today 2000;6:256–7.
2. Mansi JL, Berger U, McDonnell T, Pople A, Rayter Z, Gazet JC, et al. The fate of bone marrow micrometastases in patients with primary breast cancer. J Clin Oncol 1989;7:445–9.
3. Naume B, Zhao X, Synnestvedt M, Borgen E, Russnes HG, Lingjaerde OC, et al. Presence of bone marrow micrometastasis is associated with different recurrence risk within molecular subtypes of breast cancer. Mol Oncol 2007;1:160–71.
4. Rao G, Patel PS, Idler SP, Maloof P, Gascon P, Potian JA, et al. Facilitating role of preprotachykinin-i gene in the integration of breast cancer cells within the stromal compartment of the bone marrow: a model of early cancer progression. Cancer Res 2004;64:2874–81.
5. Riethdorf S, Wikman H, Pantel K. Review: biological relevance of disseminated tumor cells in cancer patients. Int J Cancer 2008;123:1991–2006.
6. Braun S, Pantel K. Micrometastatic bone marrow involvement: detection and prognostic significance. Med Oncol 1999;16:154–65.
7. Patel SA, Ramkissoon SH, Bryan M, Pliner LF, Dontu G, Patel PS, et al. Delineation of breast cancer cell hierarchy identifies the subset responsible for dormancy. Sci Rep 2012;2:906.
8. Aguirre-Ghiso JA. Models, mechanisms and clinical evidence for cancer dormancy. Nat Rev Cancer 2007;7:834–46.
9. Bianco P. Stem cells and bone: a historical perspective. Bone 2015;70:2–9.
10. Anthony BA, Link DC. Regulation of hematopoietic stem cells by bone marrow stromal cells. Trends Immunol 2014;35:32–7.
11. Lim PK, Bliss SA, Patel SA, Taborga M, Dave MA, Gregory LA, et al. Gap junction-mediated import of MicroRNA from bone marrow stromal cells can elicit cell cycle quiescence in breast cancer cells. Cancer Res 2011;71:1550–60.
12. Patel SA, Dave MA, Bliss SA, Giec-Ujda AB, Bryan M, Pliner LF. T_{reg}/Th17 polarization by distinct subsets of breast cancer cells is dictated by the interaction with mesenchymal stem cells. J Cancer Stem Cell 2014;2:e1003.
13. Greco SJ, Patel SA, Bryan M, Pliner LF, Banerjee D, Rameshwar P. AMD3100-mediated production of interleukin-1 from mesenchymal stem cells is key to chemosensitivity of breast cancer cells. Am J Cancer Res 2011;1:701–15.
14. Patel SA, Meyer JR, Greco SJ, Corcoran KE, Bryan M, Rameshwar P. Mesenchymal stem cells protect breast cancer cells through regulatory T cells: role of mesenchymal stem cell-derived TGF-beta. J Immunol 2010;184:5885–94.
15. Mishra PJ, Mishra PJ, Humeniuk R, Medina DJ, Alexe G, Mesirov JP, et al. Carcinoma-associated fibroblast-like differentiation of human mesenchymal stem cells. Cancer Res 2008;68:4331–9.
16. Momin EN, Vela G, Zaidi HA, Quinones-Hinojosa A. The oncogenic potential of mesenchymal stem cells in the treatment of cancer: directions for future research. Curr Immunol Rev 2010;6:137–48.
17. Bianco P, Riminucci M, Gronthos S, Robey PG. Bone marrow stromal stem cells: nature, biology, and potential applications. Stem Cells 2001;19:180–92.
18. Corselli M, Chin CJ, Parekh C, Sahaghian A, Wang W, Ge S, et al. Perivascular support of human hematopoietic stem/progenitor cells. Blood 2013;121:2891–901.
19. Arai F, Ohneda O, Miyamoto T, Zhang XQ, Suda T. Mesenchymal stem cells in perichondrium express activated leukocyte cell adhesion molecule and participate in bone marrow formation. J Exp Med 2002;195:1549–63.
20. Sakaguchi Y, Sekiya I, Yagishita K, Hinomiya K, Muneta T. Suspended cells from trabecular bone by collagenase digestion become virtually identical to mesenchymal stem cells obtained from marrow aspirates. Blood 2004;104:2728–35.
21. Thery C, Amigorena S, Raposo G, Clayton A. Isolation and characterization of exosomes from cell culture supernatants and biological fluids. Curr Protoc Cell Biol 2006;Chapter 3:Unit 3.22.
22. Edgar R, Domrachev M, Lash AE. Gene Expression Omnibus: NCBI gene expression and hybridization array data repository. Nucleic Acids Res 2002;30:207–10.
23. Arroyo JD, Chevillet JR, Kroh EM, Ruf IK, Pritchard CC, Gibson DF, et al. Argonaute2 complexes carry a population of circulating microRNAs independent of vesicles in human plasma. Proc Natl Acad Sci 2011;108:5003–8.

24. Simons M, Raposo G. Exosomes-vesicular carriers for intercellular communication. Curr Opin Cell Biol 2009;21:575–81.
25. Sohel M, Hoelker M, Noferesti SS, Salilew-Wondim D, Tholen E, Looft C, et al. Exosomal and non-exosomal transport of extra-cellular microRNAs in follicular fluid: implications for bovine oocyte developmental competence. PLoS One 2013;8:e78505.
26. Vader P, Breakefield XO, Wood MJA. Extracellular vesicles: emerging targets for cancer therapy. Trends Mol Med 2014;20:385–93.
27. Cocucci E, Meldolesi J. Ectosomes and exosomes: shedding the confusion between extracellular vesicles. Trends Cell Biol 2015;25:364–72.
28. Ono M, Kosaka N, Tominaga N, Yoshioka Y, Takeshita F, Takahashi R, et al. Exosomes from bone marrow mesenchymal stem cells contain a microRNA that promotes dormancy in metastatic breast cancer cells. Sci Signal 2014;7:ra63.
29. Liu K, Liu S, Zhang W, Ji B, Wang Y, Liu Y. miR222 regulates sorafenib resistance and enhance tumorigenicity in hepatocellular carcinoma. Int J Oncol 2014;45:1537–46.
30. Lee HK, Finniss S, Cazacu S, Xiang C, Brodie C. Mesenchymal stem cells deliver exogenous miRNAs to neural cells and induce their differentiation and glutamate transporter expression. Stem Cells Dev 2014;23:2851–61.
31. Aleynik A, Gernavage K, Mourad Y, Sherman L, Liu K, Gubenko Y, et al. Stem cell delivery of therapies for brain disorders. Clin Transl Med 2014;3:24.
32. Munoz JL, Bliss SA, Greco SJ, Ramkissoon SH, Ligon KL, Rameshwar P. Delivery of functional anti-miR-9 by mesenchymal stem cell-derived exosomes to glioblastoma multiforme cells conferred chemosensitivity. Mol Ther Nucleic Acids 2013;2:e126.
33. Gan R, Yang Y, Yang X, Zhao L, Lu J, Meng QH. Downregulation of miR-221/222 enhances sensitivity of breast cancer cells to tamoxifen through upregulation of TIMP3. Cancer Gene Ther 2014;21:290–6.
34. Munoz JL, Rodriguez-Cruz V, Greco SJ, Nagula V, Scotto KW, Rameshwar P. Temozolomide induces the production of epidermal growth factor to regulate MDR1 expression in glioblastoma cells. Mol Cancer Ther 2014;13:2399–411.
35. Moharita AL, Taborga M, Corcoran KE, Bryan M, Patel PS, Rameshwar P. SDF-1a regulation in breast cancer cells contacting bone marrow stroma is critical for normal hematopoiesis. Blood 2006;108:3245–52.
36. Hoshino A, Costa-Silva B, Shen TL, Rodrigues G, Hashimoto A, Tesic Mark M, et al. Tumour exosome integrins determine organotropic metastasis. Nature 2015;527:329–35.
37. Meacham CE, Morrison SJ. Tumour heterogeneity and cancer cell plasticity. Nature 2013;501:328–37.
38. Kreso A, Dick J. Evolution of the cancer stem cell model. Cell Stem Cell 2014;14:275–91.
39. Chaterjee M, van Golen KL. Breast cancer stem cells survive periods of farnesyl-transferase inhibitor-induced dormancy by undergoing autophagy. Bone Marrow Res 2011;2011:362938.
40. Lener T, Gioma M, Aigner L, Borger V, Buzas E, Camussi G, et al. Applying extracellular vesicles based therapeutics in clinical trials - an ISEV position paper. J Extracell Vesicles 2015;4:30087.